FORSCHUNGSZENTRUM JÜLICH GmbH
Zentralinstitut für Angewandte Mathematik
D-52425 Jülich, Tel. (02461) 61-6402

Interner Bericht

On the limit load of a square plate with an elliptical hole

Michael Heitzer

FZJ-ZAM-IB-2003-04

(letzte Änderung: 23.04.2003)

Preprint: submitted for publication

On the limit load of a square plate with an elliptical hole

Michael Heitzer

Central Institute for Applied Mathematics (ZAM),
Forschungszentrum Jülich, D–52425 Jülich, Germany

SUMMARY

The mathematical theory of plasticity is applied to the problem of a thin square plate, with an elliptical hole, yielding under loads applied at its outside edges. Lower and upper bounds to the external loads are determined for all parameters of the elliptical hole compared to the length of the side of the plate. The analytical bounds are compared to Finite Element calculations.

1. Introduction

Limit analysis is a structural mechanics method, which determines the load carrying capacity of structures. It is an important input parameter of defect assessment procedures using engineering approaches, such as the Engineering Treatment Model (ETM) developed for analysis of cracked components [16]. Therefore, the knowledge of limit loads of mechanical components and structures is useful for designers to address the modes of failure associated with the loading.

Limit loads have been obtained by analytical methods (e. g. [8], [10]), numerical methods (e. g. [18], [11], [1]) and approximation of experimental data (e. g. [16]) and the results for typical components from engineering applications are summarized for example in [13], [15], [16]. However, usually the analytical limit load of a component is not known.

The paper examines analytical lower and upper bound for the limit load of a thin square plate, with an elliptical centered hole under uniaxial, equal and opposite biaxial tension of the sides. To the authors' knowledge, no analytical bounds for this problem are published. Until know the analytical solution has to be estimated by the limit load for circular holes. It could be shown, that this gives rather poor results for the suggested loading cases.

The lower bound analysis is based on statically admissible stress fields and the upper bound analysis on discontinuous kinematically admissible velocity fields. The use of symbolic computation software was of great benefit for the solution of the corresponding nonlinear system of equations. The new lower and upper bound solutions for the limit load differ in some cases, such that it is of need to check which bound is preferable. Additional numerical Finite Element calculations for a lower bound solution with a direct method using basis reduction techniques are performed and show good agreement with the new analytical upper bounds.

2. Limit load theorems

Static theorems are formulated in terms of stress and define safe structural states giving an optimization problem for safe loads. The maximum safe load is the limit load avoiding collapse. Alternatively, kinematic theorems are formulated in terms of kinematic quantities and define unsafe structural states yielding a dual optimization problem for the minimum unsafe load. Any admissible solution to the static or kinematic theorem is a true lower or upper bound to the limit load,

respectively. Lower and upper bound converge to the same solution.

Let a structure V be loaded monotonously by the load $\boldsymbol{P} = (\boldsymbol{q}, \boldsymbol{p})$ with body forces $\boldsymbol{q}$ and surface loads $\boldsymbol{p}$. In limit analysis one is interested in the load factor $\alpha > 1$ by which $\boldsymbol{P}$ can be increased up to the collapse at $\alpha\boldsymbol{P}$.

1. **Static or lower bound theorem:**
   A structure does not collapse under a load $\alpha\boldsymbol{P}$, if an statically admissible stress field $\boldsymbol{\sigma}$ can be found, which is in equilibrium with $\alpha\boldsymbol{P}$, i. e.

$$\begin{aligned} F(\boldsymbol{\sigma}) \leq\ & \sigma_y && \text{in} \quad V, \\ \operatorname{div}\boldsymbol{\sigma} = & -\alpha\boldsymbol{q} && \text{in} \quad V, \\ \boldsymbol{\sigma}\boldsymbol{n} = & \alpha\boldsymbol{p} && \text{on} \quad \partial V_\sigma. \end{aligned} \tag{1}$$

   for the structure V, traction boundary ∂V_σ (with outer normal $\boldsymbol{n}$), yield function F, yield stress σ_y. From now on F is chosen as the square of the von Mises yield function

$$F(\boldsymbol{\sigma}) = \frac{3}{2}\boldsymbol{\sigma}^D : \boldsymbol{\sigma}^D \qquad \text{with the deviatoric stress} \qquad \boldsymbol{\sigma}^D = \boldsymbol{\sigma} - \frac{1}{3}(\operatorname{tr}\boldsymbol{\sigma})\mathbf{I}. \tag{2}$$

2. **Kinematic or upper bound theorem:**
   A structure fails by plastic collapse if there is a kinematically admissible velocity field $\dot{\boldsymbol{u}}$ and an associated strain rate field $\dot{\boldsymbol{\varepsilon}}$ such that the power of the external loads is higher than the power which can be dissipated within the structure.

$$\dot{W}_{in} = \int_V D(\dot{\varepsilon}^P)\, dV = \int_V \dot{\boldsymbol{\varepsilon}}\ \boldsymbol{\sigma}\ dV \quad \leq \quad \int_V \boldsymbol{q}\ \dot{\boldsymbol{u}}\, dV + \int_{\partial V_\sigma} \boldsymbol{p}\ \dot{\boldsymbol{u}}\, dA = \dot{W}_{ex} \tag{3}$$

$$\begin{aligned} \dot{\boldsymbol{\varepsilon}} &= \frac{1}{2}(\nabla\dot{\boldsymbol{u}} + (\nabla\dot{\boldsymbol{u}})^T) \quad \text{in } V\ , \\ \dot{\boldsymbol{u}} &= \dot{\boldsymbol{u}}_0 \qquad \text{on} \quad \partial V_u, \end{aligned} \tag{4}$$

   with boundary $\partial V = \partial V_\sigma \cup \partial V_u$.

3. Numerical solution of the lower bound approach

A lower bound of the limit load factor α_l can be calculated as the largest safety factor α which fulfills the conditions of (1). This is in the case of the von Mises yield function F a nonlinear optimization problem with the unknowns α and $\boldsymbol{\sigma}$.

$$\begin{aligned} \max \quad & \alpha \\ \text{s.t.} \quad & F(\boldsymbol{\sigma}) \leq \sigma_y^2 && \text{in } V \\ & \operatorname{div}\boldsymbol{\sigma} = -\alpha\boldsymbol{q} && \text{in } V \\ & \boldsymbol{\sigma}\,\boldsymbol{n} = \alpha\boldsymbol{p} && \text{on } \partial V_\sigma \end{aligned} \tag{5}$$

The stresses $\boldsymbol{\sigma}$ can be decomposed into fictitious elastic stresses $\boldsymbol{\sigma}^E$ and residual stresses $\boldsymbol{\rho}$ by

$$\boldsymbol{\sigma} = \boldsymbol{\sigma}^E + \boldsymbol{\rho}. \tag{6}$$

$\boldsymbol{\sigma}^E = \boldsymbol{E} : \boldsymbol{\varepsilon}$ are stresses which would appear in an infinitely elastic material for the same loading, so that the $\boldsymbol{\rho}$ result from plastic deformations. The residual stresses (eigen stresses) $\boldsymbol{\rho}$ satisfy the homogeneous static equilibrium and boundary conditions

$$\operatorname{div}\boldsymbol{\rho} = \mathbf{0} \quad \text{in } V \tag{7}$$

$$\boldsymbol{\rho}\,\boldsymbol{n} = \mathbf{0} \quad \text{on } \partial V_\sigma. \tag{8}$$

All vectors $\boldsymbol{\rho}$ which fulfill the homogeneous static equilibrium and boundary conditions define with the addition and scalar multiplication a vector space $\mathcal{B}$, the so called *residual stress space*.

The lower bound problem can be transformed into a finite optimization problem by FEM discretization. For structures with NG Gaussian points in the FEM model one has to handle $O(NG)$ unknowns and $O(NG)$ constraints. The number of Gaussian points becomes huge for realistic discretizations of industrial structures and no effective solution algorithms for discretizations of the nonlinear optimization problem (5) are available. A method for handling such large–scale optimization problems for perfect plasticity is called *basis reduction technique* or *subspace iteration* [5], [6], [7], [17], [19] and was implemented in the general purpose Finite Element Code PERMAS [5], [14].

4. Finite Element calculations

A quarter of the plate with the centered elliptical hole is discretized with 3200 nine-noded quadrilateral plane membrane elements (QUAM9 [14]) for each loading case, i. e. uniaxial, equal and opposite biaxial loading (see Fig. 1). The corresponding limit analysis optimization problems with reduced basis have up to 5 unknowns and 12800 nonlinear constraints. In Fig. 4 the fictitious elastic von Mises stresses for s=10 MPa are plotted for each loading case. All sub-figures are scaled to the highest von Mises stress which occur for opposite biaxial loading, to compare the results. The black regions show high von Mises stresses.

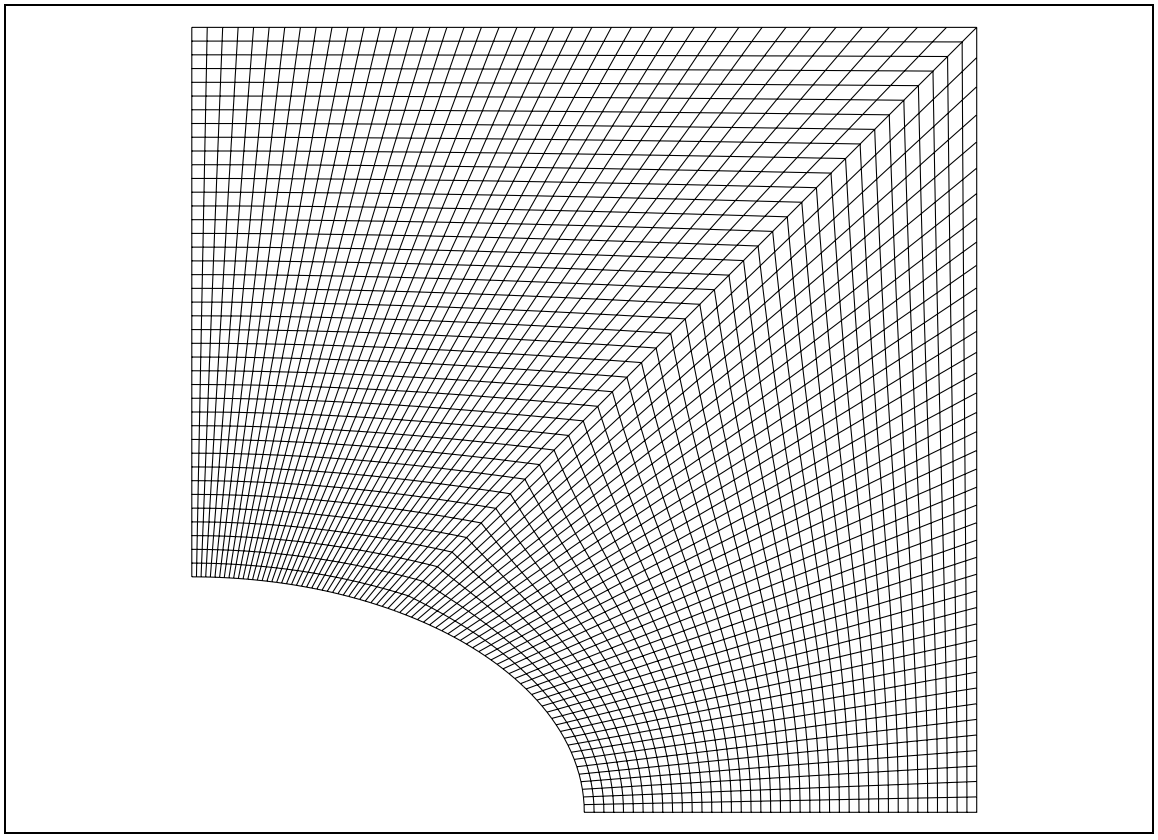

Figure 1: Finite Element mesh of the plate with an elliptical hole

(a) uniaxial load

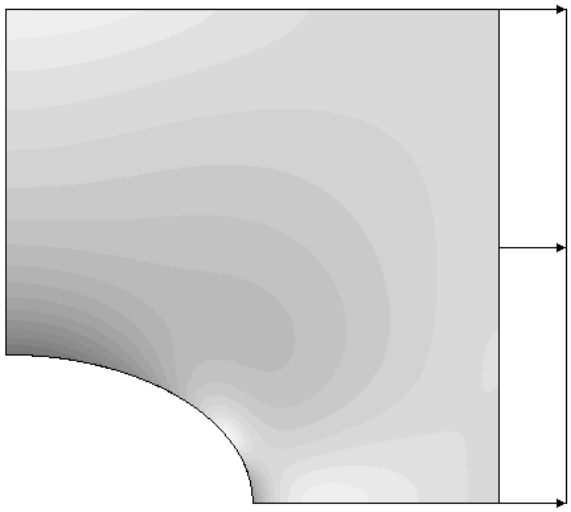

(b) equal biaxial load

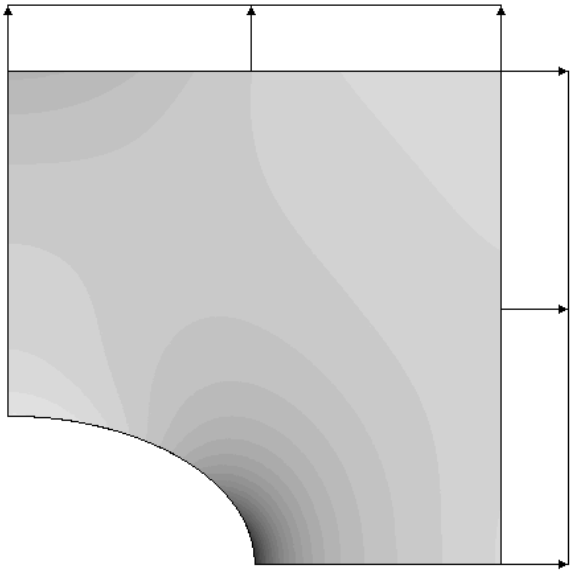

(c) opposite biaxial load

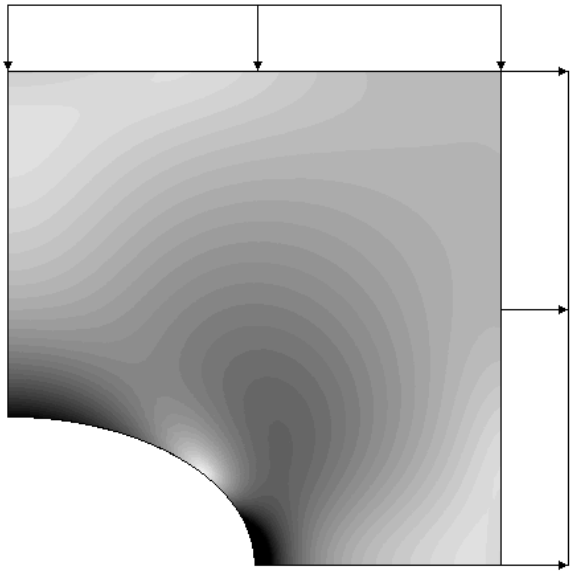

Figure 2: Elastic von Mises equivalent stresses for s=10 MPa

5. Analytical lower bound solution

A square plate with a centered elliptical hole is subjected to uniformly distributed tensile loads s and t over the two pairs of opposing ends. If the plate is uniform, collapse will occur in simple tension (t=0) for a load $s = \sigma_y$. If there is a cutout this will weaken the structure, such that it will carry a smaller load. If the cutout is defined by a circular hole, analytic lower and upper bounds are well known for Tresca and von Mises type of yield function [3], [10]. A lower bound of the limit load may be constructed by considering the discontinuous stress filed shown in Fig. 3. Each of the regions is assumed to be at constant stress, such that each region is trivially in equilibrium. Region 7 is assumed to be stress free. It remains to satisfy the boundary conditions, the stress jump conditions between the regions and the yield conditions (see [3], [10] for the special case of a circular hole). The parameters x and y have to be optimized such that the lower bound of the limit load is maximal.

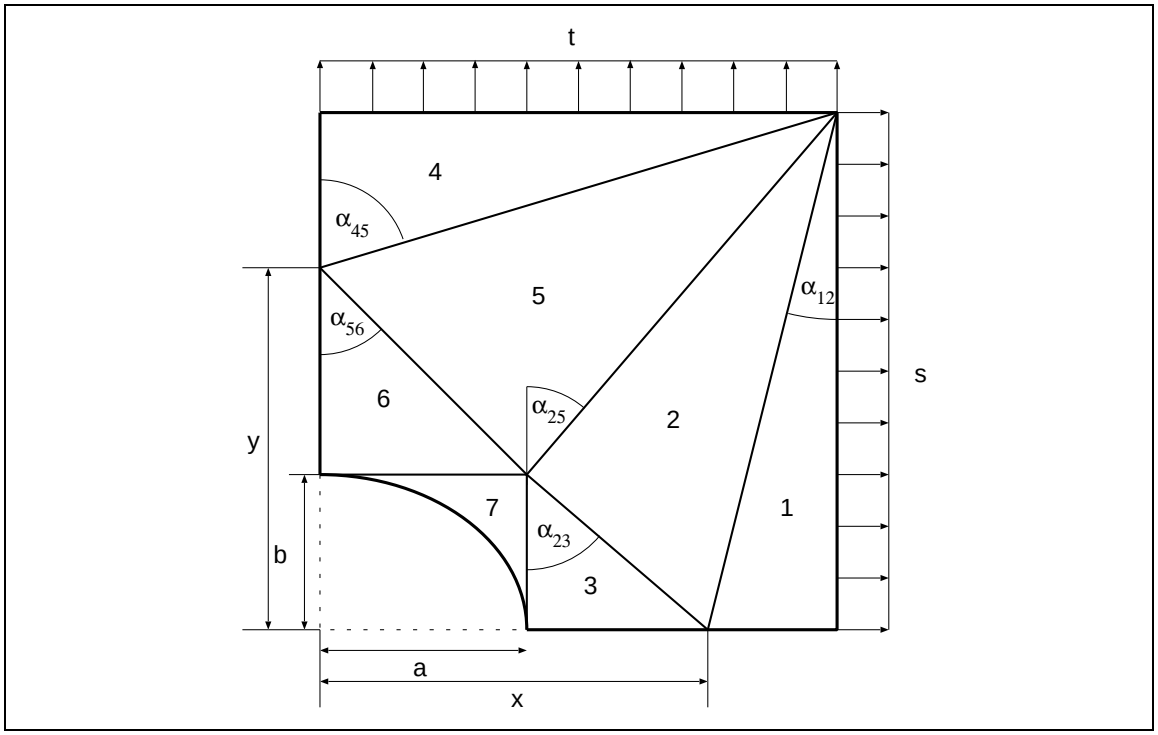

Figure 3: Definition of geometrical data and the discontinuous stress field

If the boundary of two regions i and j makes an angle α_{ij} with the y-axis, the continuity requirement for the exterior stresses may be written as [10]:

$$w_i - x_i \cos 2(\theta_i - \alpha_{ij}) = w_j - x_j \cos 2(\theta_j - \alpha_{ij}) \quad (9)$$

$$x_i \sin 2(\theta_i - \alpha_{ij}) = x_j \sin 2(\theta_j - \alpha_{ij}). \quad (10)$$

The stress variables can by transformed by

$$w_j = n_j + s_j, \;\; x_j = n_j - s_j, \;\; n_j = (w_j + x_j)/2, \;\; s_j = (w_j - x_j)/2. \quad (11)$$

In the regions 1, 3, 4 and 6 the shearing stresses vanish on a boundary and hence throughout the region, such that it holds $t_1 = t_3 = t_4 = t_6 = 0$ and $s_1 = s, s_3 = 0, n_4 = t, n_6 = 0$. From the boundary conditions it follows for the jump conditions

$$\begin{aligned} \text{Region } 1-2: \quad & w_2 - x_2 \cos 2(t_2 - \alpha_{12}) = (n_1 + s) - (n_1 - s)\cos 2\alpha_{12} \\ & x_2 \sin 2(t_2 - \alpha_{12}) = -(n_1 - s)\sin 2\alpha_{12} \\ \text{Region } 2-3: \quad & w_2 - x_2 \cos 2(t_2 - \alpha_{23}) = n_3 - n_3 \cos 2\alpha_{23} \\ & x_2 \sin 2(t_2 - \alpha_{23}) = -n_3 \sin 2\alpha_{23} \end{aligned} \quad (12)$$

$$
\begin{aligned}
\text{Region } 2-5: \qquad & w_2 - x_2\cos 2(t_2-\alpha_{25}) = w_5 - x_5\cos 2(t_5-\alpha_{25}) \\
& x_2\sin 2(t_2-\alpha_{25}) = x_5\sin 2(t_5-\alpha_{25}) \\
\text{Region } 4-5: \qquad & w_5 - x_5\cos 2(t_5-\alpha_{45}) = (t+s_4) - (t-s_4)\cos 2\alpha_{45} \\
& x_5\sin 2(t_5-\alpha_{45}) = -(t-s_4)\sin 2\alpha_{45} \\
\text{Region } 5-6: \qquad & w_5 - x_5\cos 2(t_5-\alpha_{56}) = s_6 - s_6\cos 2\alpha_{56} \\
& x_5\sin 2(t_5-\alpha_{56}) = s_6\sin 2\alpha_{56}
\end{aligned} \tag{13}
$$

The angles α_{ij} are given by the following equations:

$$
\begin{aligned}
a_{12} &:= \tan\alpha_{12} = 1-x, \qquad & a_{23} &:= \tan\alpha_{23} = \frac{a-x}{b}, \qquad & a_{25} &:= \tan\alpha_{25} = \frac{1-a}{1-b}, \\
a_{45} &:= \tan\alpha_{45} = \frac{1}{1-y}, \qquad & a_{56} &:= \tan\alpha_{56} = \frac{a}{b-y}.
\end{aligned} \tag{14}
$$

With $\phi := \tan\alpha_i$ and $\psi := \tan\alpha_j$ the following equations hold

$$
\begin{aligned}
\cos 2(\phi-\psi) &= \frac{1-\phi^2-\psi^2+\phi^2\psi^2+4\phi\psi}{(1+\phi^2)(1+\psi^2)}, \qquad & \cos 2\phi &= \frac{1-\phi^2}{(1+\phi)^2}, \\
\sin 2(\phi-\psi) &= \frac{2(\phi-\psi)(1+\phi\psi)}{(1+\phi^2)(1+\psi^2)}, \qquad & \sin 2\phi &= \frac{2\phi}{(1+\phi)^2}
\end{aligned} \tag{15}
$$

such that the jump conditions can be transformed into:

$$
\begin{aligned}
f_1 &:= w_2 - \frac{x_2(1-t_2^2-a_{12}^2+t_2^2a_{12}^2+4t_2a_{12})}{(1+t_2^2)(1+a_{12}^2)} - n_1 - s + \frac{(n_1-s)(1-a_{12}^2)}{1+a_{12}^2} \\
f_2 &:= \frac{x_2(t_2-a_{12})(1+t_2a_{12})}{1+t_2^2} + (n_1-s)a_{12} \\
f_3 &:= w_2 - \frac{x_2(1-t_2^2-a_{23}^2+t_2^2a_{23}^2+4t_2a_{23})}{(1+t_2^2)(1+a_{23}^2)} - n_3\left(1-\frac{1-a_{23}^2}{1+a_{23}^2}\right) \\
f_4 &:= \frac{x_2(t_2-a_{23})(1+t_2a_{23})}{1+t_2^2} + n_3a_{23} \\
f_5 &:= w_2 - \frac{x_2(1-t_2^2-a_{25}^2+t_2^2a_{25}^2+4t_2a_{25})}{(1+t_2^2)(1+a_{25}^2)} - w_5 + \frac{x_5(1-t_5^2-a_{25}^2+t_5^2a_{25}^2+4t_5a_{25})}{(1+t_5^2)(1+a_{25}^2)} \\
f_6 &:= \frac{x_2(t_2-a_{25})(1+t_2a_{25})}{1+t_2^2} - \frac{x_5(t_5-a_{25})(1+t_5a_{25})}{1+t_5^2} \\
f_7 &:= w_5 - \frac{x_5(1-t_5^2-a_{45}^2+t_5^2a_{45}^2+4t_5a_{45})}{(1+t_5^2)(1+a_{45}^2)} - t - s_4 + \frac{(t-s_4)(1-a_{45}^2)}{1+a_{45}^2} \\
f_8 &:= \frac{x_5(t_5-a_{45})(1+t_5a_{45})}{1+t_5^2} + (t-s_4)a_{45} \\
f_9 &:= w_5 - \frac{x_5(1-t_5^2-a_{56}^2+t_5^2a_{56}^2+4t_5a_{56})}{(1+t_5^2)(1+a_{56}^2)} - s_6\left(1+\frac{1-a_{56}^2}{1+a_{56}^2}\right) \\
f_{10} &:= \frac{x_5(t_5-a_{56})(1+t_5a_{56})}{1+t_5^2} - s_6a_{56}
\end{aligned} \tag{16}
$$

The functions $f_i, i = 1\ldots 10$ have to vanish for the analytic lower bound of the limit load for the given stress distributions. The unknowns are $n_1, w_2, x_2, n_3, s_4, t_2, w_5, t_5, x_5, s_6$. In the case of a biaxial loading with independent magnitudes $t \neq s$ the solutions are calculated using Maple 8 a

software package for symbolic and numeric computation [12] and are given by:

$$
\begin{aligned}
n_1 &= \frac{t(1-x)+bs}{(1-x)(1-a)} \\
w_2 &= \frac{sb^2-tbx+tb-sa-asx-sb+a^2s+sx-ta+xt}{(x(1-b)+b-a)(1-a)} \\
x_2 &= \frac{\sqrt{(s(b^2+ax+a-b-a^2-x)-t(bx-x-b+a))^2+4b^2s^2(1-a)^2}}{(1-a)(bx-x-b+a)} \\
t_2 &= \frac{(s(b^2+ax+a-b-a^2-x)-t(bx-x-b+a)}{sb(1-a)} \\
&- \frac{\sqrt{4s^2b^2(1-a)^2+(s(b^2+ax+a-b-a^2-x)-t(bx-x-b+a))^2}}{sb(1-a)} \\
n_3 &= \frac{t\,(x-a)-s\,b}{(x-a)\,(1-a)} \\
s_4 &= \frac{s(1-y)+at}{(1-y)(1-b)} \\
w_5 &= \frac{s(b-y-a+ay)-t(b^2-b-by+a^2-a+y)}{(ay-y+b-a)(1-b)} \\
x_5 &= \frac{\sqrt{(s(b-y-a+ay)+t(b^2-b-by-a^2+a+y))^2+4t^2a^2(1-b)^2}}{(1-b)(ay-y+b-a)} \\
\\
t_5 &= \frac{s(b-y-a+ay)+t(b^2-b-by-a^2+a+y)}{2ta(1-b)} \\
&+ \frac{\sqrt{4t^2a^2(1-b)^2+(s(b-y-a+ay)+t(b^2-b-by-a^2+a+y))^2}}{2ta(1-b)} \\
s_6 &= \frac{s(y-b)-ta}{(y-b)\,(1-b)}
\end{aligned}
\tag{17}
$$

The von Mises yield condition for region j is given by $s_j^2+n_j^2-s_jn_j \le \sigma_y^2$.

6. Uniaxial tension

6.1. Lower bound

With $n_j=\frac{w_j+x_j}{2}$ and $s_j=\frac{w_j-x_j}{2}$ for $j=1,\ldots,6$ and $t=0$ it follows from the equations (17):

$$
\begin{aligned}
n_1 &= \frac{bs}{(1-x)(1-a)} && s_1 = s \\
n_2 &= s\frac{(-b^2+a+ax+b-a^2-x)+\sqrt{(b^2+ax+a-b-a^2-x)^2+4b^2(1-a)^2}}{2(bx-x-b+a)(1-a)} \\
s_2 &= s\frac{(-b^2+a+ax+b-a^2-x)-\sqrt{(b^2+ax+a-b-a^2-x)^2+4b^2(1-a)^2}}{2(bx-x-b+a)(1-a)} \\
n_3 &= -\frac{bs}{(x-a)(1-a)} && s_3 = 0 \\
n_4 &= n_5 = n_6 = 0 && s_4 = s_5 = s_6 = \frac{s}{1-b}
\end{aligned}
\tag{18}
$$

The von Mises yield condition for region j is given by $s_j^2+n_j^2-s_jn_j \leq \sigma_y^2$ and using the definition. $v_j = 1/\sqrt{s_j^2+n_j^2-s_jn_j}$ with

$$\begin{aligned} v_1(x) &= \frac{(1-x)(1-a)}{\sqrt{b^2+(1-x)^2(1-a)^2-(1-x)(1-a)b}} \\ v_2(x) &= -\frac{(bx-x-b+a)(1-a)}{\sqrt{c}} \\ v_3(x) &= \frac{(x-a)(1-a)}{b} \\ v_4(x) &= 1-b \\ v_5(x) &= 1-b \\ v_6(x) &= 1-b \end{aligned} \tag{19}$$

with

$$\begin{aligned} c &= a^2x^2-axb-b^2x+4a^2x-2a^3x-2ax^2-ab+ba^2+x^2 \\ &\quad -2ax+2b^2a^2+bx+b^4-2b^3-2a^3+a^4-5b^2a+b^2ax+4b^2+a^2 \end{aligned} \tag{20}$$

the conditions for the lower bound are transformed into $s/\sigma_y \leq v_j(x), j = 1,\ldots,6$. The yield functions dependent only on the parameter x, such that in this case the stresses in region 4, 5 and 6 are identical and the regions can be joined (see also the definition of the stress regions in [3], [10]). The functions $v_2(x)$ and $v_3(x)$ are monotone increasing and $v_1(x)$ is monotone decreasing in the interval of possible solutions of $v_1(x) = v_2(x)$ and $v_1(x) = v_3(x)$. Therefore the best lower bound is given by $v_1(x^*)$, where $x^* = \max\{x_1, x_2\}$ is the greater solution of $v_1(x_1) = v_2(x_1)$ and $v_1(x_2) = v_3(x_2)$. Fig. 4 and 5 are different diagrams to show the dependence of the limit load on the parameters a and b. In addition, the known solution for the circular hole [3] under uniaxial tension is added. Fig. 4 shows contour lines for constant b. For $b \leq 0.2$ it can be seen, that the limit load is the same for all $a \leq b$, such that it corresponds to the solution of the circular hole with radius b. The limit load for $a \leq b$ is dominated for a large range by the solution $1-b$. For $a > b$ the value $1-b$ seems to be a bad estimate.

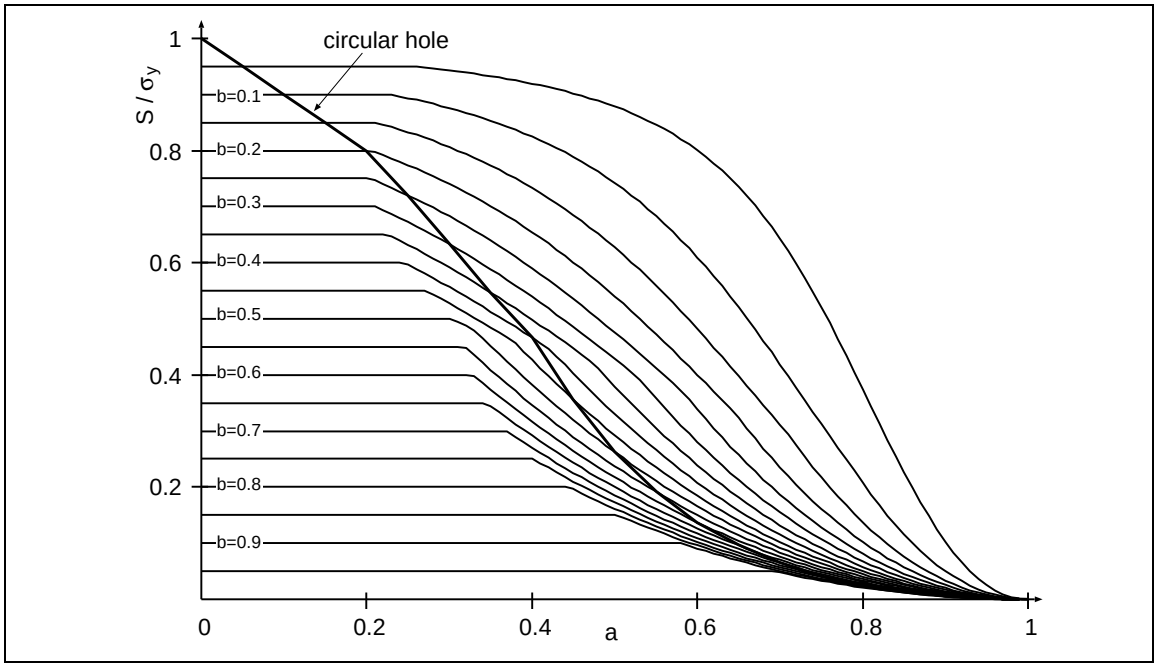

Figure 4: Analytic lower bounds for constant b.

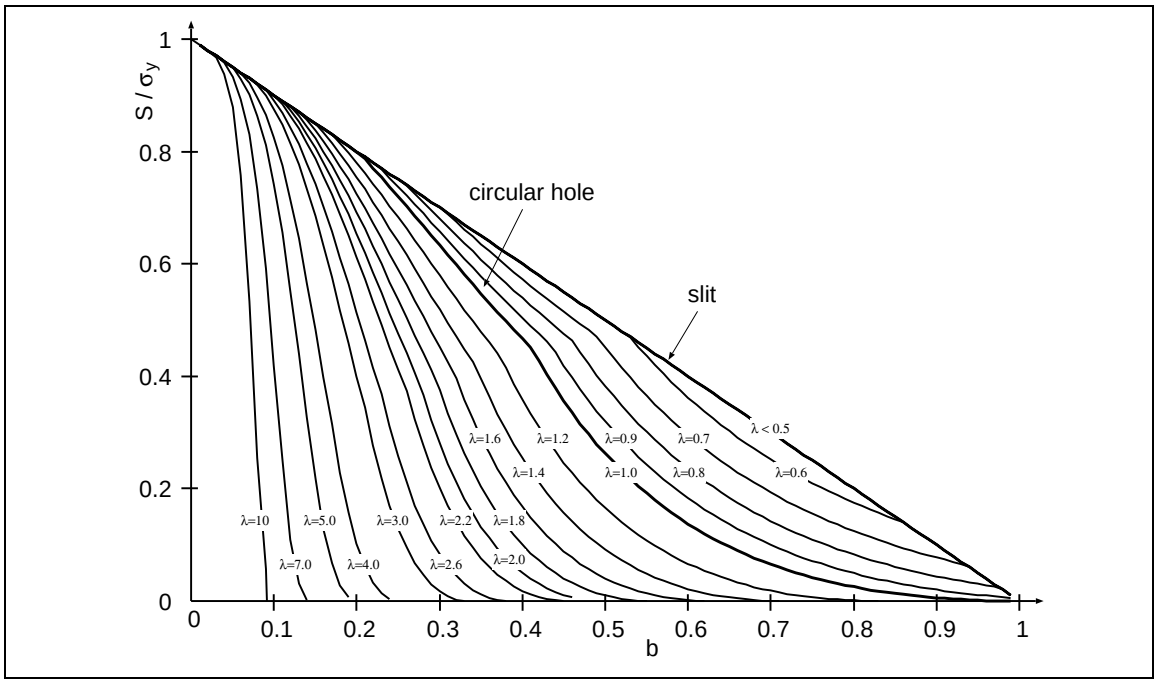

Figure 5: Analytic lower bounds for constant $\lambda = a/b$.

6.2. Upper bound

This upper bound analysis of the limit load is based on assumed simple deformation mechanisms and a rigid-plastic material model. Every deformation mode which is compatible with the velocity boundary conditions leads to an upper bound of the limit load [8]. The internal rate of working in a local neck is given by [9]:

$$\int k\, v\, \sqrt{1 + 3\sin^2\psi}\, ds \tag{21}$$

where v is the velocity with which the parts of the plate slide relative to each other and k is $\sigma/2$ or $\sigma/\sqrt{3}$ for Tresca and von Mises yield criterion, respectively. v is inclined at an angle ψ to the neck and the integral is evaluated along the neck. Therefore, the internal rate of working W_I can be calculated with the length of the plastic mechanism l_m by

$$W_I = k\, v\, \sqrt{1 + 3\sin^2\psi}\, l_m \tag{22}$$

In this case a pair of straight necks run from the unstressed edge of the plate and meet on the edge of the elliptical hole (see Fig. 6(a)). The remainder of the plate remains rigid (see also [3], [11]) and hence from (22) follows

$$W_I = \frac{4\sigma_y}{\sqrt{3}} \frac{\sqrt{1 + 3\sin^2\psi}}{\sin\beta}(1-b)v. \tag{23}$$

The external rate of working W_E is given by

$$W_E = 4sv\cos(\beta - \psi), \tag{24}$$

such that the upper bound follows from $W_I \geq W_E$ and is given by:

$$s \leq \frac{\sqrt{1 + 3\sin^2\psi}}{\sqrt{3}\sin\beta\cos(\beta-\psi)}(1-b)\sigma_y. \tag{25}$$

This bound has a minimum value if $\psi = \sin^{-1}(1/3)$ and $\beta = \frac{\pi}{4} + \frac{\psi}{2}$ and is given by

$$s \leq (1-b)\sigma_y. \tag{26}$$

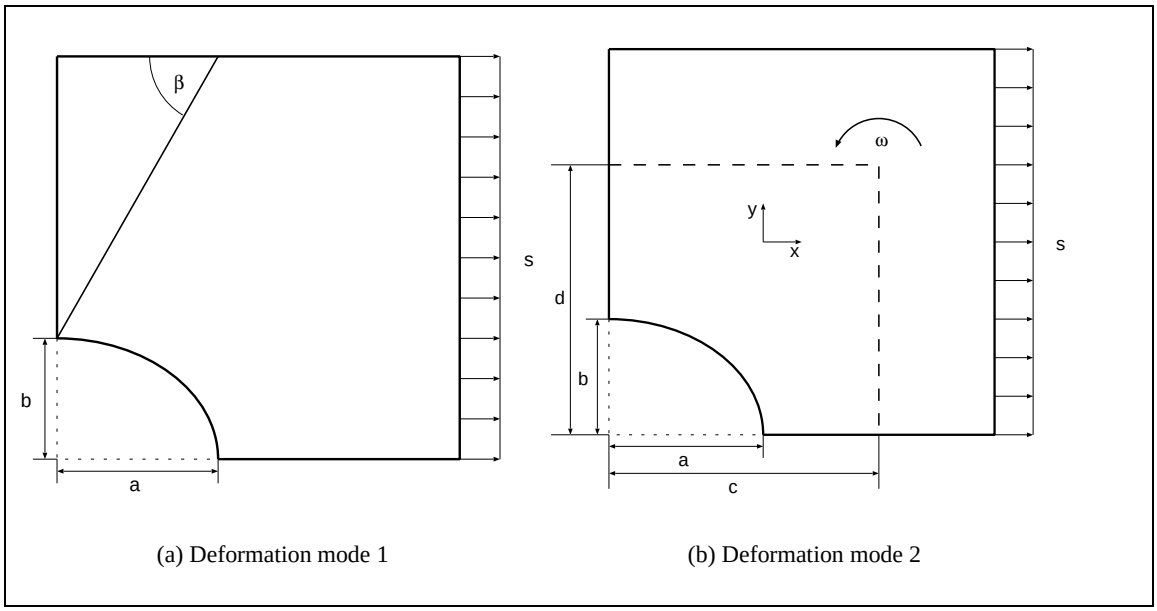

(a) Deformation mode 1 (b) Deformation mode 2

Figure 6: Deformation modes for upper bound solution

The second upper bound is derived from the deformation mode in which the four quarters of the plate rotate with angular velocity ω about points $(\pm c, \pm d)$ with local necking or bulging along the axes (see Fig. 6(b)). There is a normal discontinuity of velocity whose magnitude is $2\omega(x-c)$ and $2\omega(y-d)$ at the points $(x,0)$ and $(0,y)$, respectively and the remainder of the plate is rigid. The associated stress normal to the axis is $\pm 2\sigma_y/\sqrt{3}$ at each point in the deforming region [3]. Therefore, the internal rate of working W_I can be calculated by

$$\begin{aligned} W_I &= \frac{2\sigma_y}{\sqrt{3}}\left[\int_a^c \omega(x-c)\,dx + \int_c^1 \omega(x-c)\,dx + \int_b^d \omega(y-d)\,dx + \int_d^1 \omega(y-d)\,dx\right] \\ &= \frac{\sigma_y}{\sqrt{3}}\omega\left[(a-c)^2 + (1-c)^2 + (b-d)^2 + (1-d)^2\right] \\ &= \frac{2\sigma_y}{\sqrt{3}}\omega\left[\frac{a^2+b^2}{2} + c^2 + d^2 + 1 - (a+1)c - (b+1)d\right] \end{aligned} \tag{27}$$

which tends for the circular hole ($a=b$) to the known solution [3]:

$$W_I^c = \frac{2\sigma_y}{\sqrt{3}}\omega\left[a^2 + c^2 + d^2 + 1 - (a+1)(c+d)\right] \tag{28}$$

The external rate of working W_E is given by integration along the loaded side of the plate

$$W_E = \left|\int_0^1 s\omega(y-d)\,dy\right| = s\omega\left(d - \frac{1}{2}\right) \tag{29}$$

such that the upper bound follows from $W_I \geq W_E$ and is given by:

$$s \leq \frac{a^2 + b^2 + 2\left\{c^2 + d^2 + 1 - (a+1)c - (b+1)d\right\}}{\sqrt{3}\left(d - \frac{1}{2}\right)}\sigma_y. \tag{30}$$

The least value of the upper bound occurs when the plate is in equilibrium [3], [4], i.e. the stresses along the boundary of the deforming region are in equilibrium with the load s. Parallel to the x-axis it is

$$0 = -\frac{2\sigma_y}{\sqrt{3}}(c-a) + \frac{2\sigma_y}{\sqrt{3}}(1-c) = \frac{2\sigma_y}{\sqrt{3}}(1+a-2c) \tag{31}$$

and parallel to the y-axis

$$s = \frac{2\sigma_y}{\sqrt{3}}(d-b) - \frac{2\sigma_y}{\sqrt{3}}(1-d) = \frac{2\sigma_y}{\sqrt{3}}(2d-b-1) \tag{32}$$

and taking the moments about the center of the hole with $\sigma_\theta = \pm 2\sigma_y/\sqrt{3}$

$$\begin{aligned} s &= 2\left\{\int_a^c r\sigma_\theta\, dr + \int_c^1 r\sigma_\theta\, dr \int_b^d r\sigma_\theta\, dr + \int_d^1 r\sigma_\theta\, dr\right\} \\ &= \frac{4\sigma_y}{\sqrt{3}}\left(\frac{c^2-a^2}{2} - \frac{1-c^2}{2} + \frac{d^2-b^2}{2} - \frac{1-d^2}{2}\right) = \frac{2\sigma_y}{\sqrt{3}}(2c^2+2d^2-(2+a^2+b^2)) \end{aligned} \tag{33}$$

From eqs. (31)-(33) it follows for the limit load s^*

$$s^* \le \frac{2}{\sqrt{3}}\left(\sqrt{a^2+2b^2+2-2b-2a}-b\right)\sigma_y \tag{34}$$

which tends for the circular hole to the known solution (see [3]).
For $a \ge 1 - \frac{1}{2}\sqrt{-1-4\sqrt{3}b^2+2b+4\sqrt{3}b-b^2}$ eq. (34) gives a better upper bound than eq. (26), for example for $b = 0.8$, $a \ge 0.4832$ or $b = 0.5$, $a \ge 0.3913$.

6.3. Finite Element calculations

For comparison the direct limit analysis using the basis reduction technique is chosen, the results are given in the following figures. The Finite Element lower bound calculations are closer to the analytical upper bound, such that this bound seems to be the more realistic one. A rough estimation of the lower and upper bound using the solution of a plate with a circular hole of radius $\max\{a,b\}$ for the lower bound and $\min\{a,b\}$ for the upper bound gives rather poor results (see Fig. 7(j)).

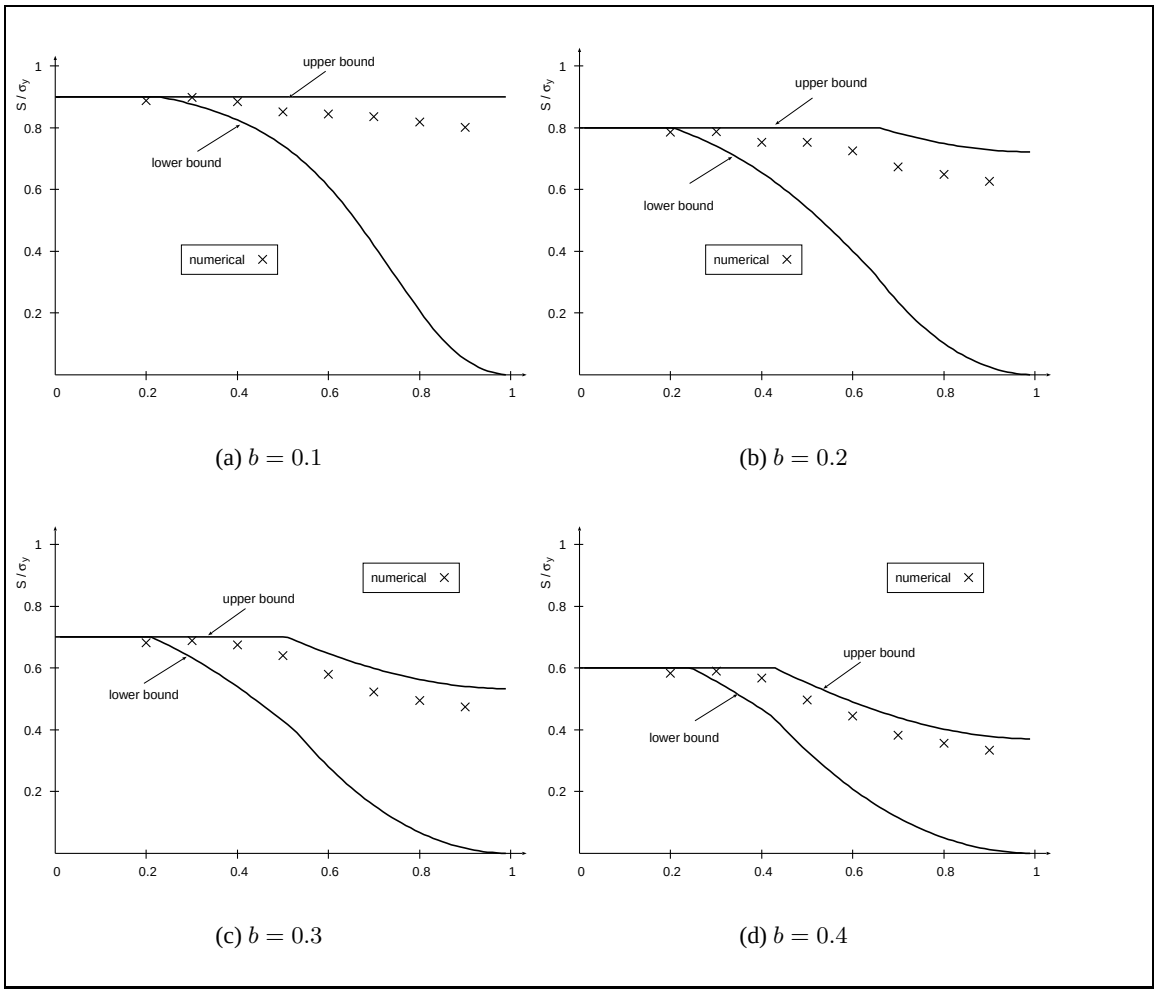

(a) $b = 0.1$ (b) $b = 0.2$

(c) $b = 0.3$ (d) $b = 0.4$

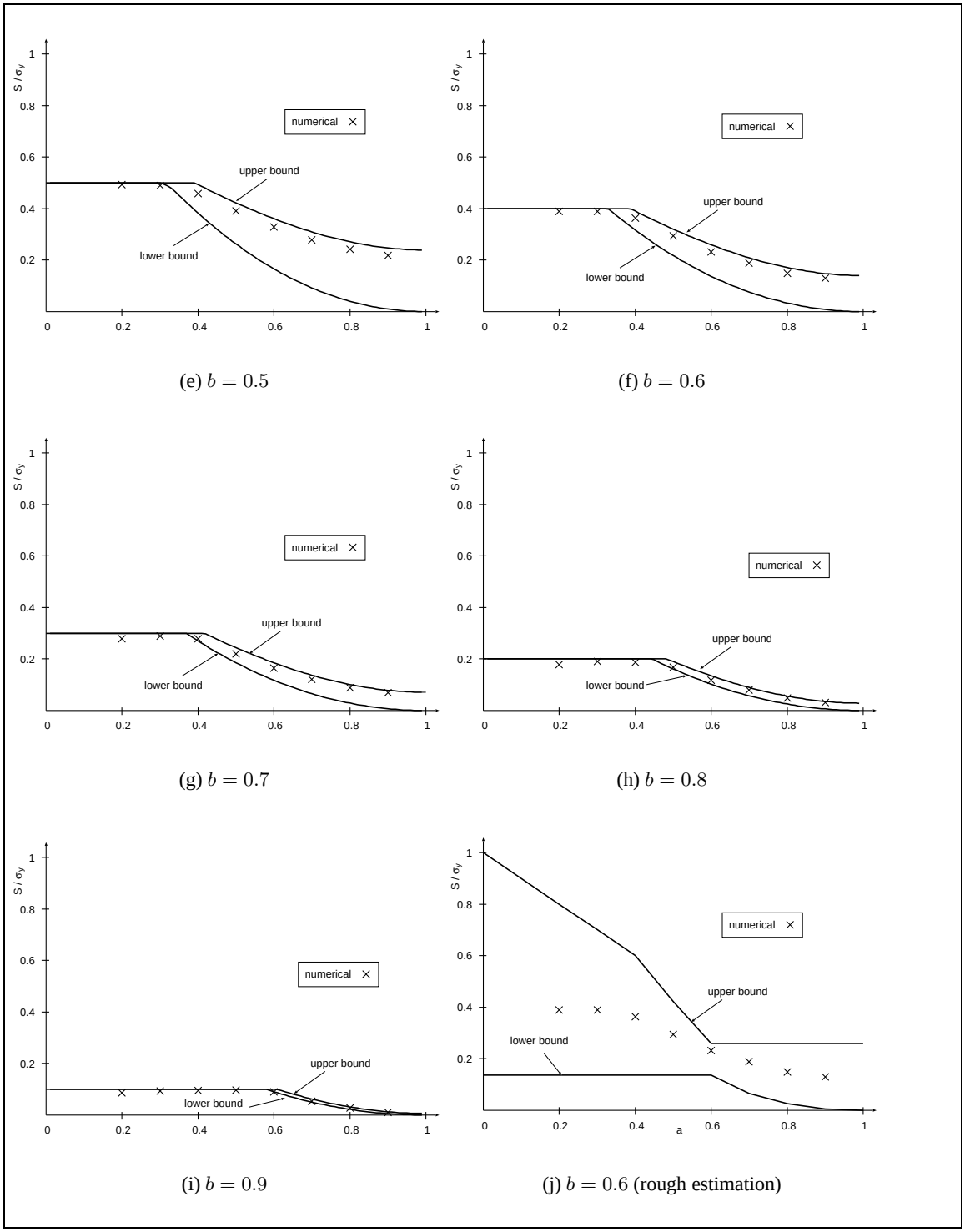

(e) $b = 0.5$ (f) $b = 0.6$

(g) $b = 0.7$ (h) $b = 0.8$

(i) $b = 0.9$ (j) $b = 0.6$ (rough estimation)

Figure 7: Comparison of lower and upper bounds for uniaxial loading with Finite Element calculations for constant b and rough estimation for $b = 0.6$

7. Equal biaxial tension

7.1. Lower bound

A lower bound can be derived following the investigations shown in [3], [8]. In plane stress in the plastic region the characteristics of the differential equations of stress are two families of curves inclined at angles $\pm(\pi/4 + \psi/2)$ to the direction of the algebraically greater principal stress [8] with

$$3 \sin \psi = \frac{\sigma_1 + \sigma_2}{\sigma_1 - \sigma_2}, \quad \sigma_1 \geq \sigma_2 \tag{35}$$

and the principal stresses are given with the auxiliary angle φ by

$$\sigma_{1,2} = \sigma_y \sin(\varphi \pm \pi/6), \quad \varphi \geq \pi/6. \tag{36}$$

The characteristics are real if and only if $|\sigma_1 + \sigma_2| \leq 3|\sigma_1 - \sigma_2|$.

A lower bound for all possible values of the parameters of the ellipse is given by the stress distribution given in Fig. 8 (see [3] for a similar distribution).

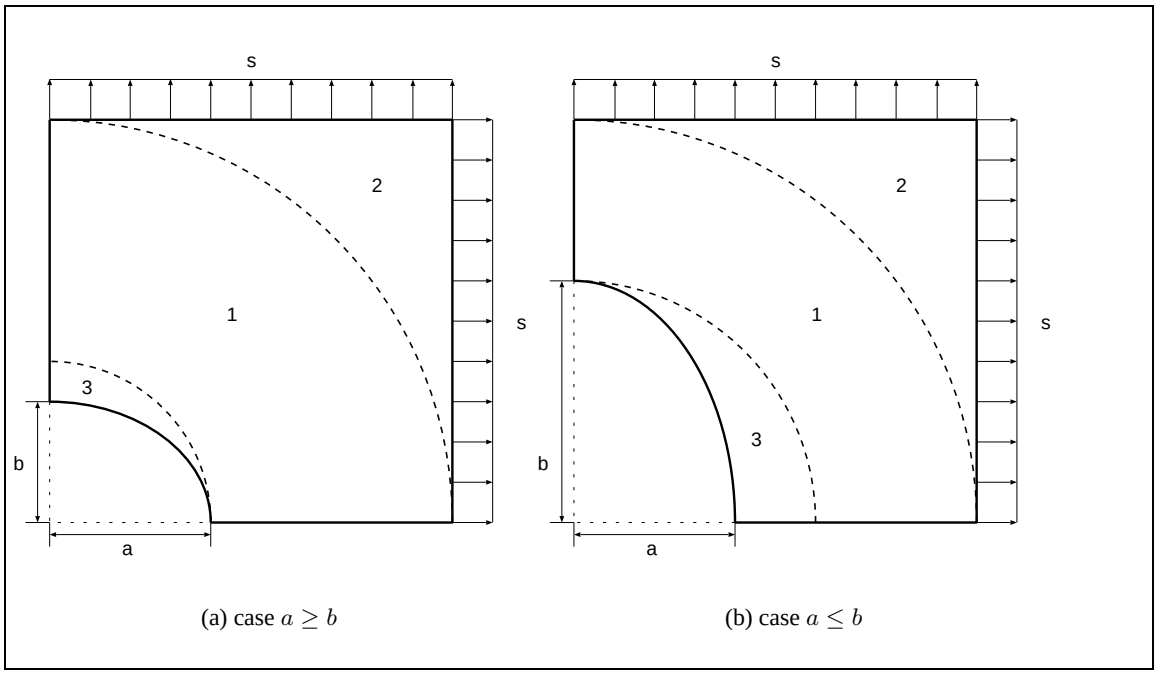

(a) case $a \geq b$ (b) case $a \leq b$

Figure 8: Discontinuous stress field for biaxial tension

In the annulus between the hole and the circle touching the side of the plate (region 1), the stress is assumed to be axially symmetric. For an axially symmetric plane stress distribution with stresses σ_r and σ_θ the equilibrium equations are given by:

$$\frac{\partial \sigma_r}{\partial r} = \frac{\sigma_\theta - \sigma_r}{r}. \tag{37}$$

With

$$\sigma_r = \frac{2}{\sqrt{3}} \sigma_y \sin\left(\varphi - \frac{\pi}{6}\right) \quad \text{and} \quad \sigma_\theta = \frac{2}{\sqrt{3}} \sigma_y \sin\left(\varphi + \frac{\pi}{6}\right) \tag{38}$$

and

$$\sigma_\theta - \sigma_r = \frac{2}{\sqrt{3}} \sigma_y \cos \varphi \tag{39}$$

the equilibrium equations are

$$\cos\left(\varphi - \frac{\pi}{6}\right) \frac{\partial \varphi}{\partial r} = \frac{\cos \varphi}{r}. \tag{40}$$

The solution of this differential equation with a constant c is given by [8]:

$$r^2 \cos\varphi = c^2 e^{\sqrt{3}\varphi} \tag{41}$$

In the case of a circular hole with radius a and $\varphi = \pi/6$ on the plastic boundary $r = a$ it holds

$$2r^2 \cos\varphi = \sqrt{3} a^2 e^{\sqrt{3}(\varphi - \pi/6)}. \tag{42}$$

With the condition $|\sigma_1 + \sigma_2| \leq 3|\sigma_1 - \sigma_2|$ and the definition (38) the characteristics of the differential equations are real if and only if $|\sin\varphi| \leq 3|\cos\varphi|$, i.e. $0 \leq \varphi \leq \pi/3$.

On the boundaries between the regions the normal stress σ_r is continuous but the tangential stress σ_θ is discontinuous. Region 3 is stress free ($\sigma_1 = \sigma_2 = 0$) and region 2 is uniformly stressed below the yield point in equal biaxial stressing:

$$\sigma_1 = \sigma_2 = \frac{2}{\sqrt{3}} \sigma_y \sin\left(\alpha - \frac{\pi}{6}\right) \tag{43}$$

with

$$2\cos\alpha = \sqrt{3} a^2 e^{\sqrt{3}(\alpha - \pi/6)}, \tag{44}$$

such that $\alpha = \pi/2$ and $\alpha = \pi/6$ correspond to $a = 0$ and $a = 1$, respectively.

The von Mises stresses in the regions are given by:

$$\text{region1} \quad : \quad \sigma_{vm} = \sqrt{\sigma_r^2 + \sigma_\theta^2 - \sigma_r \sigma_\theta} = \sigma_y \tag{45}$$

$$\text{region2} \quad : \quad \sigma_{vm} = \sqrt{\sigma_1^2 + \sigma_2^2 - \sigma_1 \sigma_2} = \frac{2}{\sqrt{3}} \sigma_y \sin\left(\alpha - \frac{\pi}{6}\right). \tag{46}$$

This stress distribution fulfills the equilibrium conditions for all $b \leq a$, such that a lower bound of the limit load s^* is given by the lower bound of the circular hole [3]:

$$s^* \geq \frac{2}{\sqrt{3}} \sigma_y \sin\left(\alpha - \frac{\pi}{6}\right). \tag{47}$$

By changing a and b, a lower bound for the limit load s^* for equal biaxial loading is also valid for $b \geq a$. The results for this function are plotted together with the estimation of Amstutz & Seegers [16] for constant b in Fig.9

7.2. Estimation from experimental data

An estimation for the limit load in plane stress for a plate with a centered crack of length a loaded by s perpendicular to the crack and by λs parallel to the crack direction is given by Amstutz & Seeger in [2], [16]:

$$s_{lim} = \frac{\sigma_y (1-a)}{\sqrt{1 - \lambda(1-a) + \lambda^2 (1-a)^2}}. \tag{48}$$

The solution results from the constant principal stress field:

$$\sigma_1 = \lambda s, \;\; \sigma_2 = \frac{s}{1-a}, \sigma_{vm} = \frac{s\sqrt{1 - \lambda(1-a) + \lambda^2(1-a)^2}}{1-a}. \tag{49}$$

This stress distribution does not fulfill the boundary condition of a stress free crack and thus gives only an approximation and not a true lower bound for the limit load. Nevertheless the comparison with experimental data show good agreement [16]. For the case of biaxial loading ($\lambda = 1$) and uniaxial loading ($\lambda = 0$) this gives for plane stress:

$$\text{biaxial}: \; s_{lim} = \frac{\sigma_y (1-a)}{\sqrt{1 - a + a^2}} \quad \text{uniaxial}: \; s_{lim} = \sigma_y (1-a). \tag{50}$$

The results of both bounds are illustrated in Fig. (9), see also [13], [15], [16], [18], for limit load solutions for plane structures.

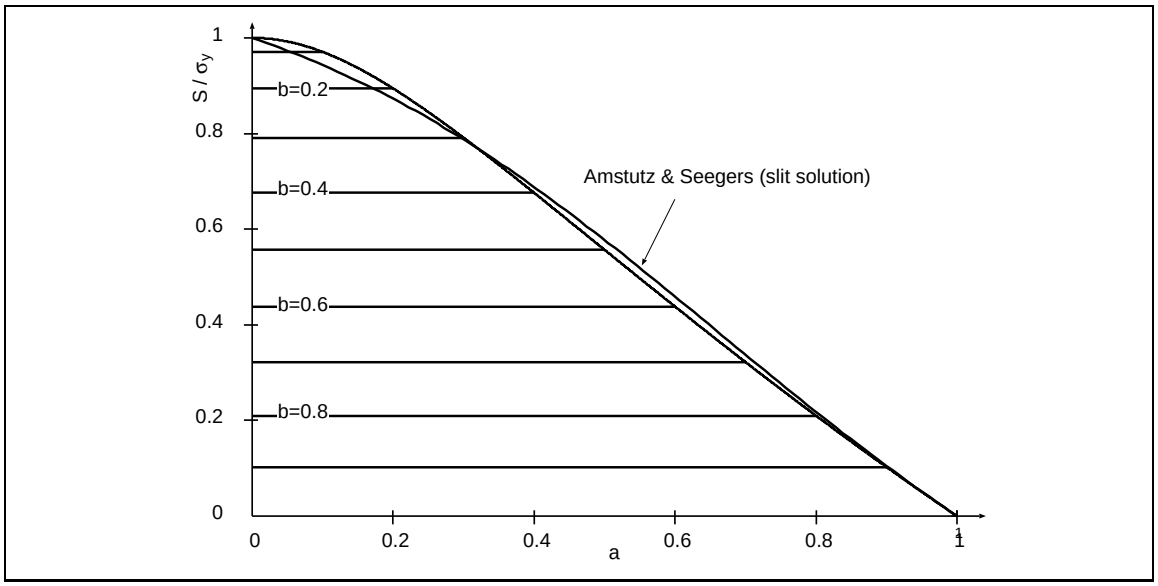

Figure 9: Analytic lower bounds for equal biaxial loading for constant a with slit solution $\frac{(1-a)}{\sqrt{1-a+a^2}}$.

7.3. Upper bound

Deformation mode 1

In the first mode deformation occurs only in the necks and the material is rigid on each side of the neck. Hence with the notation of Fig. 10 the internal rate of working W_I is given with the boundary equation of the elliptical hole

$$\left(\frac{x}{a}\right)^2 + \left(\frac{y}{b}\right)^2 = 1, \tag{51}$$

and the length of the plastic mechanism l_m

$$l_m = \frac{\sqrt{a^2 + b^2\tan^2(\phi)} - ab}{\sin(\beta)\sqrt{a^2 + b^2\tan^2(\phi)}} \tag{52}$$

such that with the velocity v (see eq. (22)):

$$W_I = \frac{v\sigma_y}{\sqrt{3}}\sqrt{1+3\sin^2(\psi)}\; l_m = \frac{v\sigma_y\sqrt{1+3\sin^2(\psi)}}{\sqrt{3}}\frac{\sqrt{a^2 + b^2\tan^2(\phi)} - ab}{\sin(\beta)\sqrt{a^2 + b^2\tan^2(\phi)}} \tag{53}$$

The external rate of working W_E depends on the length $\overline{AB}$:

$$\overline{AB} = \frac{ab}{\sqrt{b^2 + a^2\cot^2(\phi)}} + \cos(\beta)l_m, \tag{54}$$

such that the external rate of working W_E is given by:

$$W_E = s\; v\;\left(\cos(\beta-\psi) - \sin(\beta-\psi)\overline{AB}\right) \tag{55}$$

From eqs. (52)-(55) follows, that an upper bound for the limit load s^* is given for all β, ϕ, ψ by

$$\begin{aligned} s^* &\leq \frac{l_m\sqrt{1+3\sin^2(\psi)}}{\sqrt{3}\left(\cos(\beta-\psi) - \sin(\beta-\psi)\overline{AB}\right)}\sigma_y \\ &= \frac{\sqrt{1+3\sin^2(\psi)}\left(\sqrt{a^2 + b^2\tan^2(\phi)} - ab\right)}{\sqrt{3}\left[\sqrt{a^2 + b^2\tan^2(\phi)}\sin(\psi) + ab\sin(\beta-\psi)\left(\cos(\beta) - \sin(\beta)\sqrt{\frac{a^2+b^2\tan^2(\phi)}{b^2+a^2\cot^2(\phi)}}\right]\right)}\sigma_y \\ &= \frac{\sqrt{1+3\sin^2(\psi)}\,(c_1 - ab)}{\sqrt{3}\left[c_1\sin(\psi) + ab\sin(\beta-\psi)\left(\cos(\beta) - \sin(\beta)\frac{c_1}{c_2}\right]\right)}\sigma_y, \end{aligned} \tag{56}$$

with $c_1 = \sqrt{a^2 + b^2 \tan^2(\phi)}$ and $c_2 = \sqrt{b^2 + a^2 \cot^2(\phi)}$, which tends for the case of a circular hole ($a = b$) to (see [3]).

$$s_c^* \leq \frac{\sqrt{1 + 3\sin^2(\psi)}\,(1 - a\cos(\phi))}{\sqrt{3}\,[\sin(\psi) + a\sin(\beta - \psi)\cos(\beta + \psi)]} \tag{57}$$

A simple approximation of eq. (56) is given by setting $\beta = \psi = \pi/2$, such that it holds

$$s^* \leq \frac{2}{\sqrt{3}} \frac{c_1 - ab}{c_1} = \frac{2}{\sqrt{3}} \frac{\sqrt{a^2 + b^2 \tan^2(\phi)} - ab}{\sqrt{a^2 + b^2 \tan^2(\phi)}} \tag{58}$$

and by setting $\phi = 0$ it holds

$$s^* \leq \frac{2}{\sqrt{3}}(1 - b) \;\text{ and also by symmetry }\; s^* \leq \frac{2}{\sqrt{3}}(1 - a). \tag{59}$$

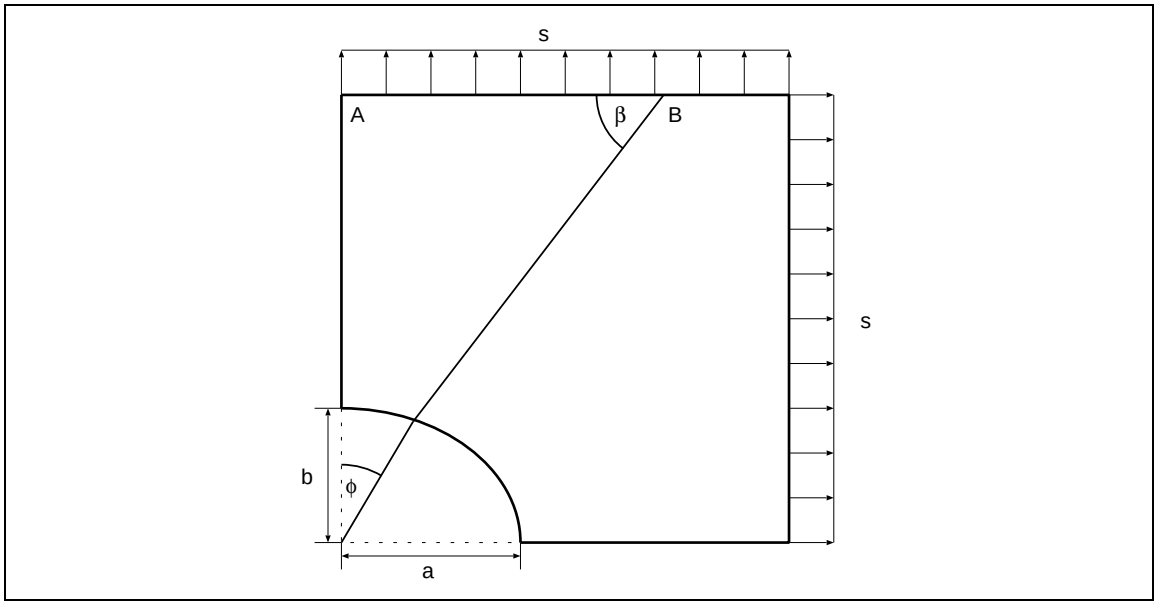

Figure 10: Deformation mode for upper bound solution for equal biaxial loading

Deformation mode 2

An upper bound of the limit load s^* is given by the uniform deformation of the plate (see [3]). The external rate of working W_E is given with the normal velocity U of each edge independent of the shape of the hole:

$$W_E = 8sU. \tag{60}$$

With the area $A = \pi ab$ of the elliptical hole, the internal rate of working W_I is given by:

$$W_I = 2\sigma_y U(4 - \pi ab). \tag{61}$$

Using $W_I \geq W_E$ an upper bound for the limit load s^* and is given by:

$$s^* \leq \left(1 - \frac{\pi ab}{4}\right) \sigma_y. \tag{62}$$

7.4. Finite Element calculations

In the equal biaxial loading case the solutions are symmetrical with respect to a and b, such that the results of the lower bound are plotted only for constant b. The comparison between lower and upper bound for parameters a and b shows, that the limit behavior is dominated by the behavior of a plate with circular hole of radius $\max\{a, b\}$.

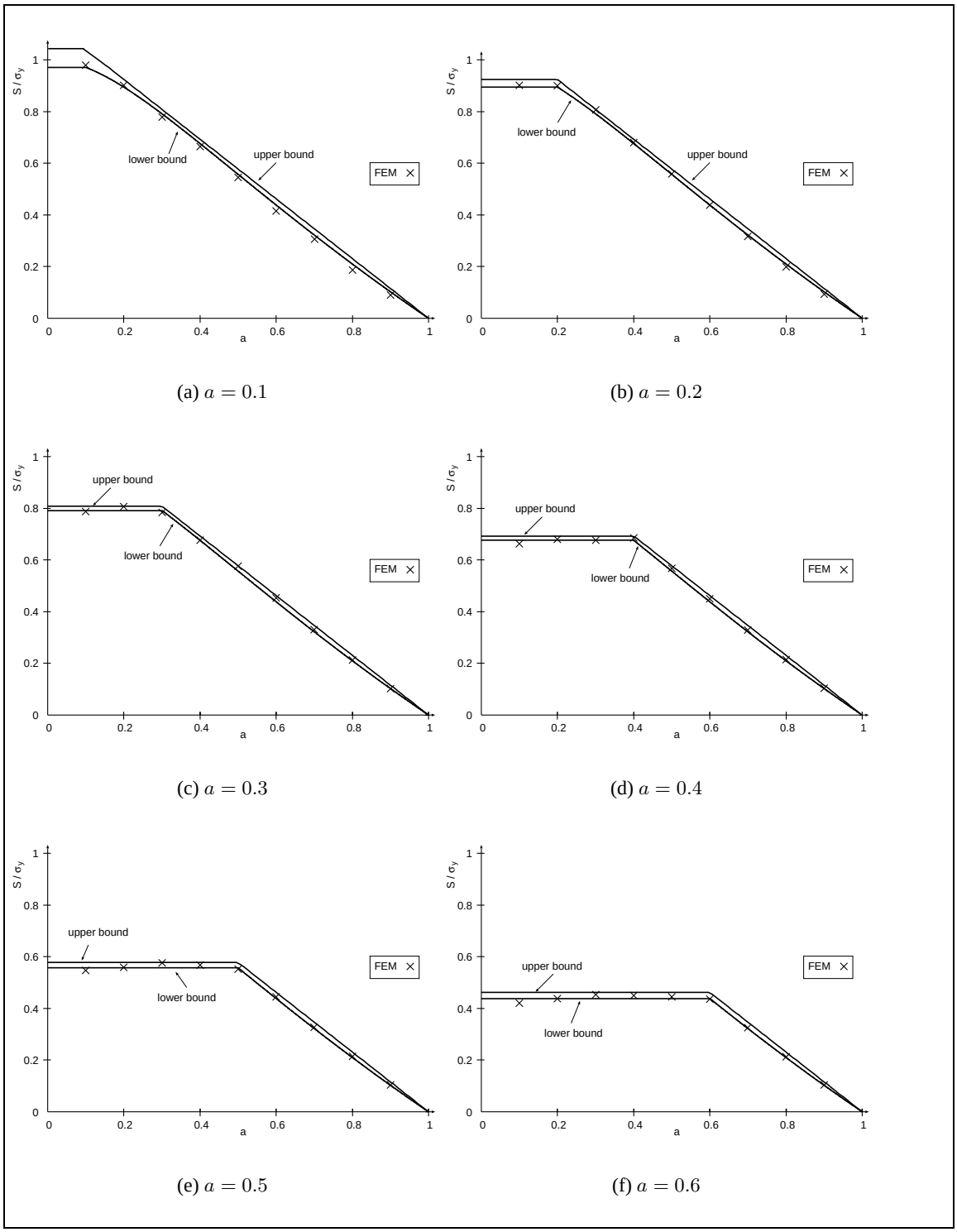

(a) $a = 0.1$ (b) $a = 0.2$

(c) $a = 0.3$ (d) $a = 0.4$

(e) $a = 0.5$ (f) $a = 0.6$

Figure 11: Comparison of lower and upper bounds for equal biaxial loading with Finite Element calculations for constant a

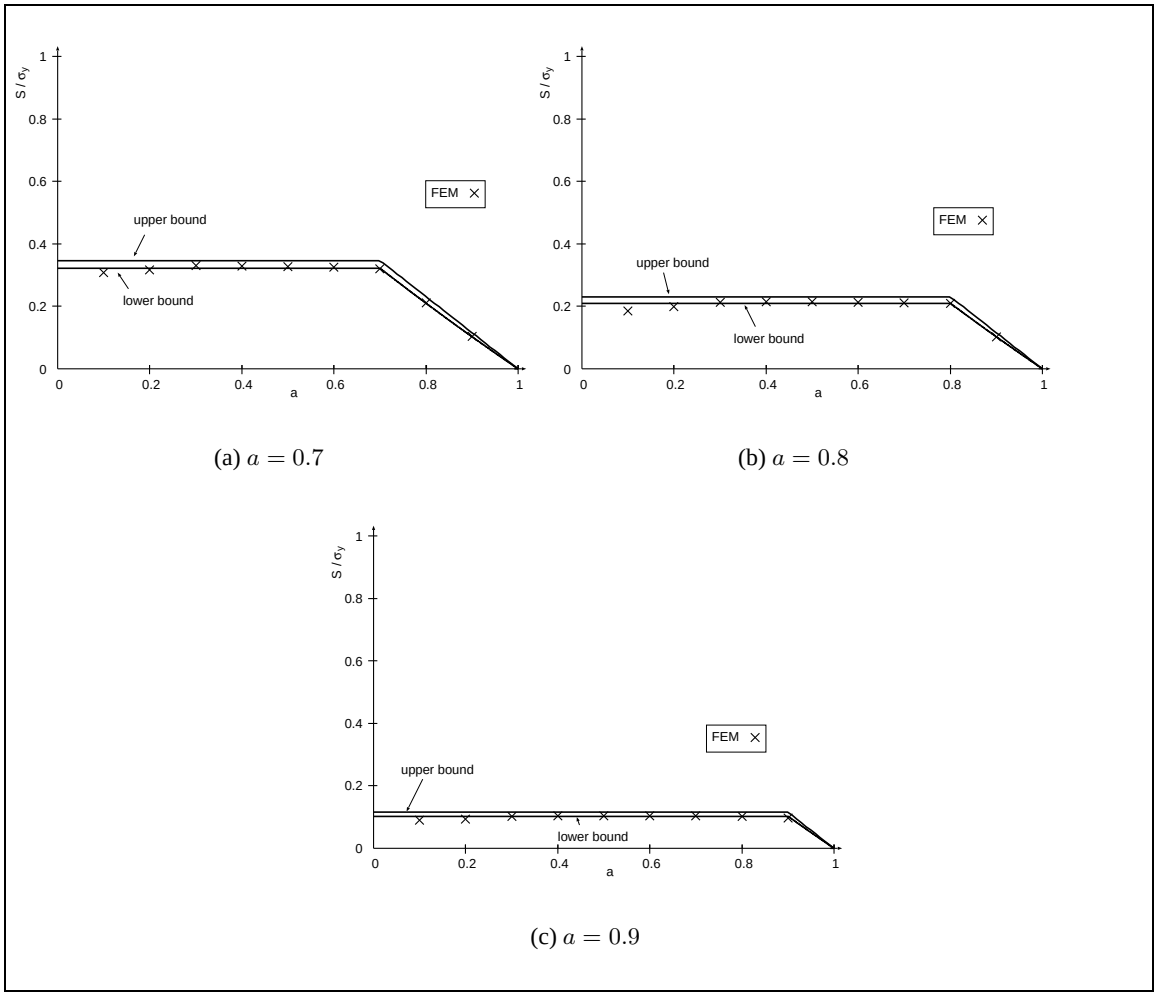

(a) $a = 0.7$

(b) $a = 0.8$

(c) $a = 0.9$

Figure 12: Comparison of lower and upper bounds for equal biaxial loading with Finite Element calculations for constant b

8. Opposite biaxial loading

8.1. Lower bound

With $n_j = \frac{w_j + x_j}{2}$ and $s_j = \frac{w_j - x_j}{2}$ for $j = 1, \ldots, 6$ and $t = -s$ it follows from the equations (17):

$$\begin{aligned}
n_1 &= s\frac{b+x-1}{(1-x)(1-a)} \\
w_2 &= s\frac{a^2+b^2+bx-ax-2b}{-(1-a)(bx-x-b+a)} \\
x_2 &= s\frac{\sqrt{(b^2-a^2+ax+bx+2a-2b-2x)^2+4b^2(1-a)^2}}{(1-a)(bx-x-b+a)} \\
n_3 &= \frac{s(a-b-x)}{(x-a)\,(1-a)} \\
s_4 &= \frac{s(1-y-a)}{(1-y)(1-b)} \\
w_5 &= \frac{s(a^2+b^2+ay-by-2a)}{(1-b)(ay-y+b-a)} \\
x_5 &= \frac{s\sqrt{(b^2-a^2-by-ay+2a-2b+2y)^2+4a^2(1-b)^2}}{(1-b)(ay-y+b-a)} \\
s_6 &= \frac{s(y-b+a)}{(y-b)\,(1-b)}
\end{aligned} \tag{63}$$

Using $n_j^2 + s_j^2 - n_j s_j = \frac{w_j^2+3x_j^2}{4}$, the conditions of the lower bound for the 6 regions are given by:

$$\begin{aligned}
s &\leq \frac{(1-x)(1-a)\sigma_y}{\sqrt{(1-x)^2(1-a)^2+(1-x-b)^2+(1-x)(1-a)(1-x-b)}} \\
s &\leq \frac{2(1-a)|bx-x-b+a|\sigma_y}{\sqrt{(a^2+b^2+bx-ax-2b)^2+3(b^2-a^2+ax+bx+2a-2b-2x)^2+12b^2(1-a)^2}} \\
s &\leq \frac{(x-a)(1-a)\sigma_y}{|x-a+b|} \\
s &\leq \frac{(1-y)(1-b)\sigma_y}{\sqrt{(1-y)^2(1-b)^2+(1-y-a)^2+(1-y-a)(1-y)(1-b)}} \\
s &\leq \frac{2(1-b)|ay-y+b-a|\sigma_y}{\sqrt{(a^2+b^2+ay-by-2a)^2+3(b^2-a^2-ay-by+2a-2b+2y)^2+12a^2(1-b)^2}} \\
s &\leq \frac{(y-b)(1-b)\sigma_y}{|y-b+a|}
\end{aligned} \tag{64}$$

The functions v_1, v_2 and v_3 dependent only on x and the functions v_4, v_5 and v_6 dependent only on y. The best lower bound of s^* is given by $s^* \geq \min\{s_x, s_y\}$ with

$$\begin{aligned}
s_x &= \min\{v_1(x), v_2(x), v_3(x)\} \quad x \in [a, 1] \\
s_y &= \min\{v_4(y), v_5(y), v_6(y)\} \quad y \in [b, 1].
\end{aligned}$$

The values s_x and s_y are given by the intersections between the corresponding functions and are calculated using Maple 8 a software package for symbolic and numeric computation [12].

8.2. Upper bound

Deformation mode 1

In the first mode the four quarters of the plate rotate with angular velocity ω about points $(\pm c, \pm d)$ with local necking or bulging along the axes (see Fig. 6(a)).

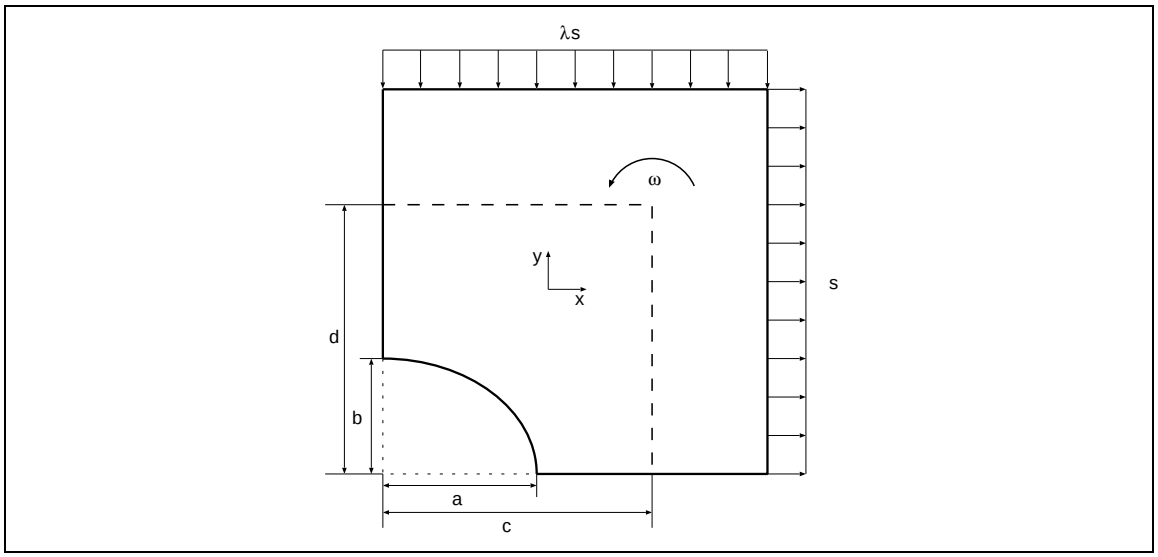

Figure 13: Deformation mode 1 for opposite biaxial loading

There is a normal discontinuity of velocity whose magnitude is $2\omega(x-c)$ and $2\omega(y-d)$ at the points $(x,0)$ and $(0,y)$, respectively and the remainder of the plate is rigid. The associated stress normal to the axis is $\pm 2\sigma_y/\sqrt{3}$ at each point in the deforming region [3]. Therefore, the internal rate of working W_I can be calculated with the length of the plastic mechanism l_m by

$$\begin{aligned} W_I &= \frac{2\sigma_y}{\sqrt{3}}\left[\int_a^c \omega(x-c)\,dx + \int_c^1 \omega(x-c)\,dx + \int_b^d \omega(y-d)\,dx + \int_d^1 \omega(y-d)\,dx\right] \\ &= \frac{\sigma_y}{\sqrt{3}}\omega\left[(a-c)^2 + (1-c)^2 + (b-d)^2 + (1-d)^2\right] \\ &= \frac{2\sigma_y}{\sqrt{3}}\omega\left[\frac{a^2+b^2}{2} + c^2 + d^2 + 1 - (a+1)c - (b+1)d\right] \end{aligned} \tag{65}$$

which tends for the circular hole ($a=b$) to the known solution [3]:

$$W_I^c = \frac{2\sigma_y}{\sqrt{3}}\omega\left[a^2 + c^2 + d^2 + 1 - (a+1)(c+d)\right] \tag{66}$$

The external rate of working W_E is given by integration along the loaded side of the plate

$$W_E = \left|\int_0^1 s\omega(y-d)\,dy\right| - \left|\int_0^1 \lambda s\omega(x-c)\,dy\right| = s\omega\left((d-\lambda c) - \frac{1}{2}(1-\lambda)\right) \tag{67}$$

such that the upper bound follows from $W_I \geq W_E$ and is given by:

$$s^* \leq \frac{a^2+b^2+2\left\{c^2+d^2+1-(a+1)c-(b+1)d\right\}}{\sqrt{3}\left((d-\lambda c) - \frac{1}{2}(1-\lambda)\right)}\sigma_y. \tag{68}$$

The least value of the upper bound occurs when the plate is in equilibrium [3], [4], i.e. the stresses along the boundary of the deforming region are in equilibrium with the load s. Parallel to the x-axis it is

$$\lambda s = -\frac{2\sigma_y}{\sqrt{3}}(c-a) + \frac{2\sigma_y}{\sqrt{3}}(1-c) = \frac{2\sigma_y}{\sqrt{3}}(1+a-2c) \tag{69}$$

and parallel to the y-axis

$$s = \frac{2\sigma_y}{\sqrt{3}}(d-b) - \frac{2\sigma_y}{\sqrt{3}}(1-d) = \frac{2\sigma_y}{\sqrt{3}}(2d-b-1) \tag{70}$$

and taking the moments about the center of the hole with $\sigma_\theta = \pm 2\sigma_y/\sqrt{3}$

$$\begin{aligned} s(1-\lambda) &\leq 2\left\{\int_a^c r\sigma_\theta\, dr + \int_c^1 r\sigma_\theta\, dr \int_b^d r\sigma_\theta\, dr + \int_d^1 r\sigma_\theta\, dr\right\} \\ &= \frac{4\sigma_y}{\sqrt{3}}\left(\frac{c^2-a^2}{2} - \frac{1-c^2}{2} + \frac{d^2-b^2}{2} - \frac{1-d^2}{2}\right) \\ &= \frac{2\sigma_y}{\sqrt{3}}(2c^2+2d^2-(2+a^2+b^2)) \end{aligned} \tag{71}$$

From eqs. (69)-(71) it follows for the limit load s^*

$$s^* \leq \frac{2}{\sqrt{3}} \frac{\lambda a - b + \sqrt{2\lambda^2 a^2 - 2\lambda ab + 2b^2 + 2\lambda^2 - 2\lambda^2 a + \lambda^2 b^2 - 2\lambda^2 b + 2 - 2a + a^2 - 2b}}{1+\lambda^2} \tag{72}$$

which gives in the case of opposite biaxial loading case ($\lambda = -1$)

$$s^* \leq \frac{1}{\sqrt{3}}\left(\sqrt{3a^2+3b^2+2ab+4-4a-4b} - a - b\right)\sigma_y \tag{73}$$

which is symmetrical in a and b. Especially for circular holes ($a = b$) (see [3]) holds:

$$s_c^* \leq \frac{2}{\sqrt{3}}(\sqrt{2a^2-2a+1} - a)\sigma_y \tag{74}$$

Deformation mode 2

The plate is supposed to have a velocity discontinuity of magnitude v in each quarter of the plate (see Figs. 14(a) and 14(b)), depending on the shape of the elliptical hole. The material is rigid on each side of the neck. With the notation of Figs. 14(a) and 14(b) and the boundary equation of the elliptical hole

$$\left(\frac{x}{a}\right)^2 + \left(\frac{y}{b}\right)^2 = 1, \tag{75}$$

the length of the plastic mechanism l_m^a and l_m^b of mode (a) and (b), respectively can be calculated:

$$\begin{aligned} l_m^a &= \frac{\sqrt{a^2 + b^2\tan^2(\phi_a)} - ab}{\sin(\beta_a)\sqrt{a^2+b^2\tan^2(\phi_a)}} \\ l_m^b &= \frac{\sqrt{b^2 + a^2\tan^2(\phi_b)} - ab}{\sin(\beta_b)\sqrt{b^2+a^2\tan^2(\phi_b)}} \end{aligned} \tag{76}$$

The internal rate of working W_I in each quarter for both modes can be calculated with l_m^a and l_m^b

$$\begin{aligned} W_I^a &= v\,\frac{\sigma_y}{\sqrt{3}} l_m^a = \frac{\sqrt{a^2 + b^2\tan^2(\phi_a)} - ab}{\sqrt{3}\sin(\beta_a)\sqrt{a^2+b^2\tan^2(\phi_a)}}\, v\,\sigma_y \\ W_I^b &= v\,\frac{\sigma_y}{\sqrt{3}} l_m^b = \frac{\sqrt{b^2 + a^2\tan^2(\phi_a)} - ab}{\sqrt{3}\sin(\beta_b)\sqrt{b^2+a^2\tan^2(\phi_b)}}\, v\,\sigma_y \end{aligned} \tag{77}$$

The external rate of working W_E depends on the length $\overline{AB}$ with:

$$\begin{aligned} \overline{AB}_a &= \frac{ab}{\sqrt{b^2 + a^2\cot^2(\phi_a)}} + \cos(\beta_a) l_m^a, \\ \overline{AB}_b &= \frac{ab}{\sqrt{a^2 + b^2\cot^2(\phi_b)}} + \cos(\beta_b) l_m^b \end{aligned} \tag{78}$$

such that the external rate of working W_E is given by:

$$W_E^{a,b} = s\, v\ \left(\cos(\beta_{a,b}) + \sin(\beta_{a,b})\overline{AB}_{a,b}\right) \tag{79}$$

and an upper bound and is given by $\min\{s_a, s_b\}$ for all β, ϕ with:

$$s_{a,b} = \frac{l_m^{a,b}}{\sqrt{3}\left(\cos(\beta_{a,b}) + \sin(\beta_{a,b})\overline{AB}_{a,b}\right)}\sigma_y. \tag{80}$$

From eqs. (77), (79) and (80) follows that the bound s_b can be obtained by exchanging the parameters a and b in the definition of s_a. Therefore an upper bound of the limit load s^* is given by (using the abbreviation $\beta = \beta_a$ and $\phi = \phi_a$):

$$s^* \leq \frac{\sqrt{a^2 + b^2\tan^2(\phi)} - ab}{\sqrt{3}\left(\sin(2\beta)\sqrt{a^2 + b^2\tan^2(\phi)} - ab\sin(\beta)\left[\cos(\beta) - \sin(\beta)\sqrt{\frac{a^2 + b^2\tan^2(\phi)}{b^2 + a^2\cot^2(\phi)}}\right]\right)}\sigma_y, \tag{81}$$

which becomes independent of b for $a = 0$ with $\beta = \pi/4$ and $s_a = 1/\sqrt{3}$. In the case of a circular hole ($a = b$) the solutions give the same results [3].

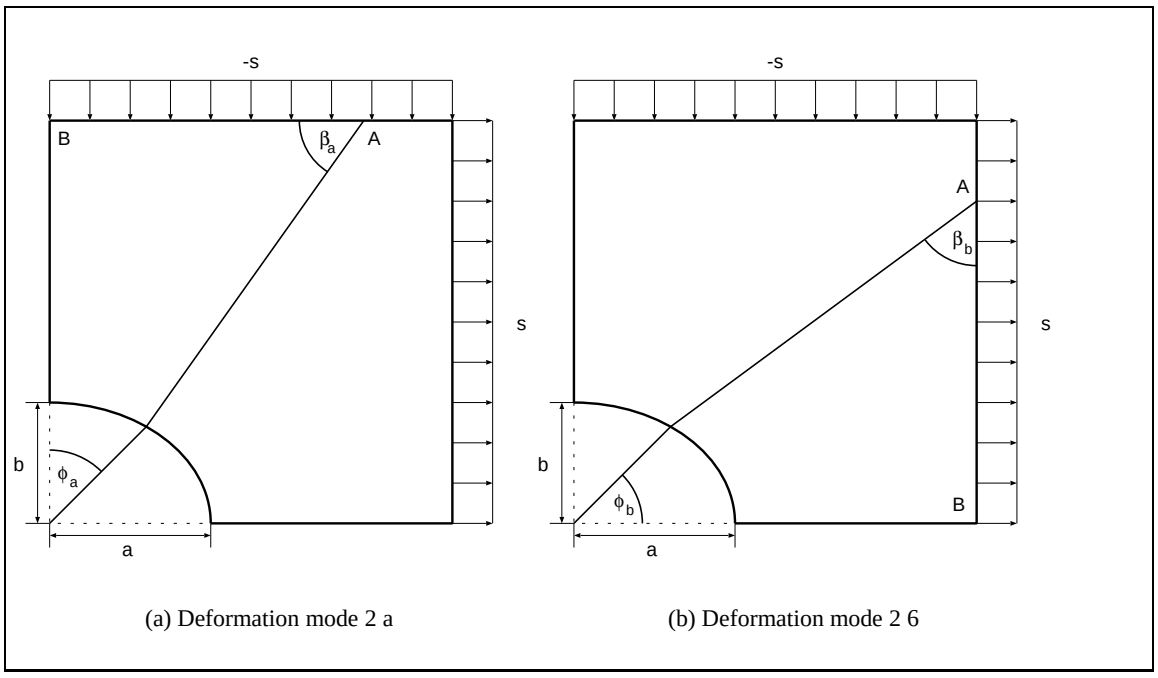

(a) Deformation mode 2 a

(b) Deformation mode 2 6

Figure 14: Deformation modes for the upper bound solution

8.3. Finite Element calculations

For comparison the direct limit analysis using the basis reduction technique is chosen (see the previous section). The results are given in the following figures. In this loading case the solutions are symmetrical with respect to a and b, such that the comparison is plotted only for constant b. The Finite Element lower bound calculations are closer to the analytical upper bound, such that this bound seems to be the more realistic one. For $b > 0.4$ the difference between the lower and the upper bound is minimal for the case of a circular hole ($a = b$) and for the degenerated cases $a = 0$ and $a = 1$.

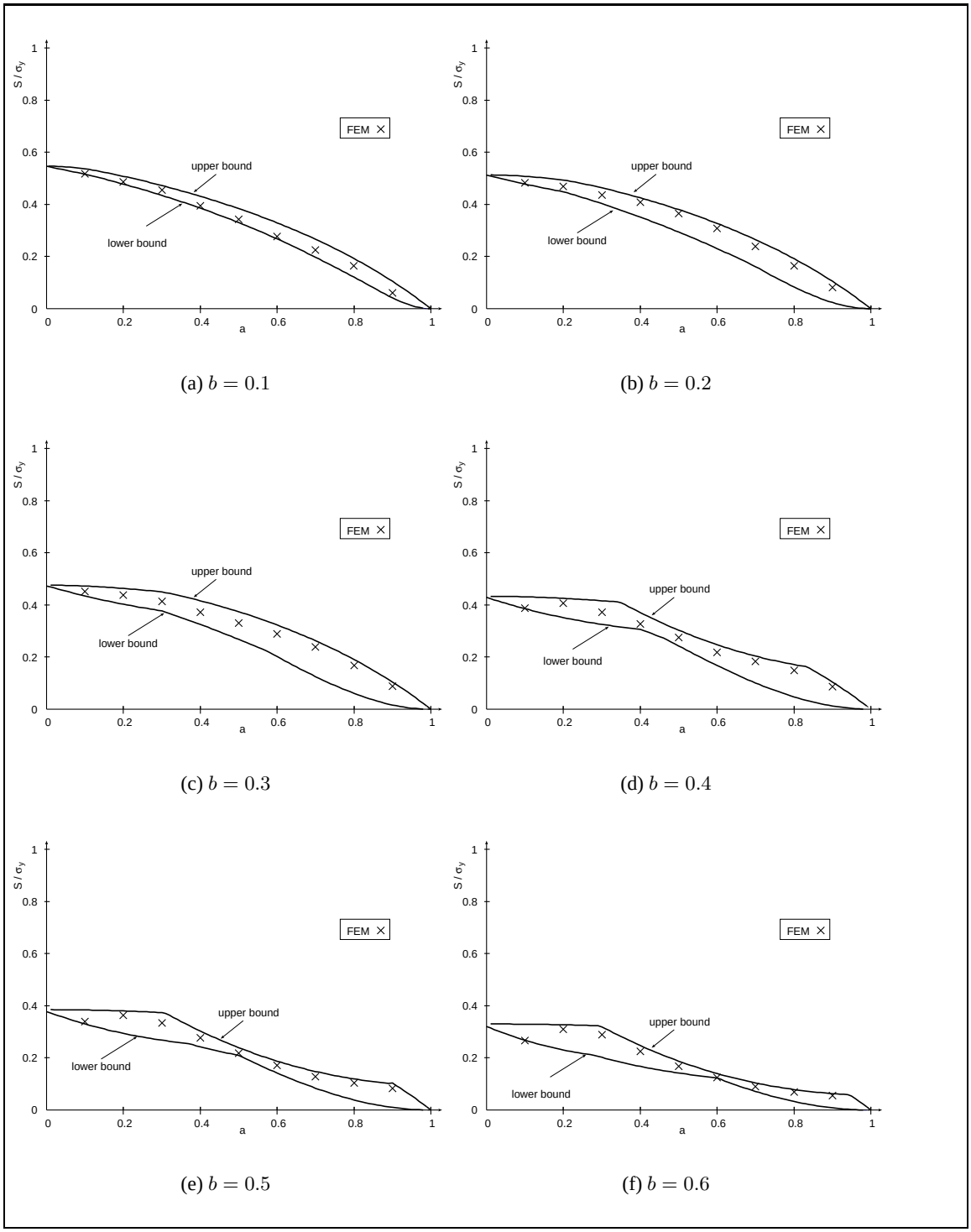

(a) $b = 0.1$

(b) $b = 0.2$

(c) $b = 0.3$

(d) $b = 0.4$

(e) $b = 0.5$

(f) $b = 0.6$

Figure 15: Comparison of lower and upper bounds for opposite biaxial loading with Finite Element calculations for constant b

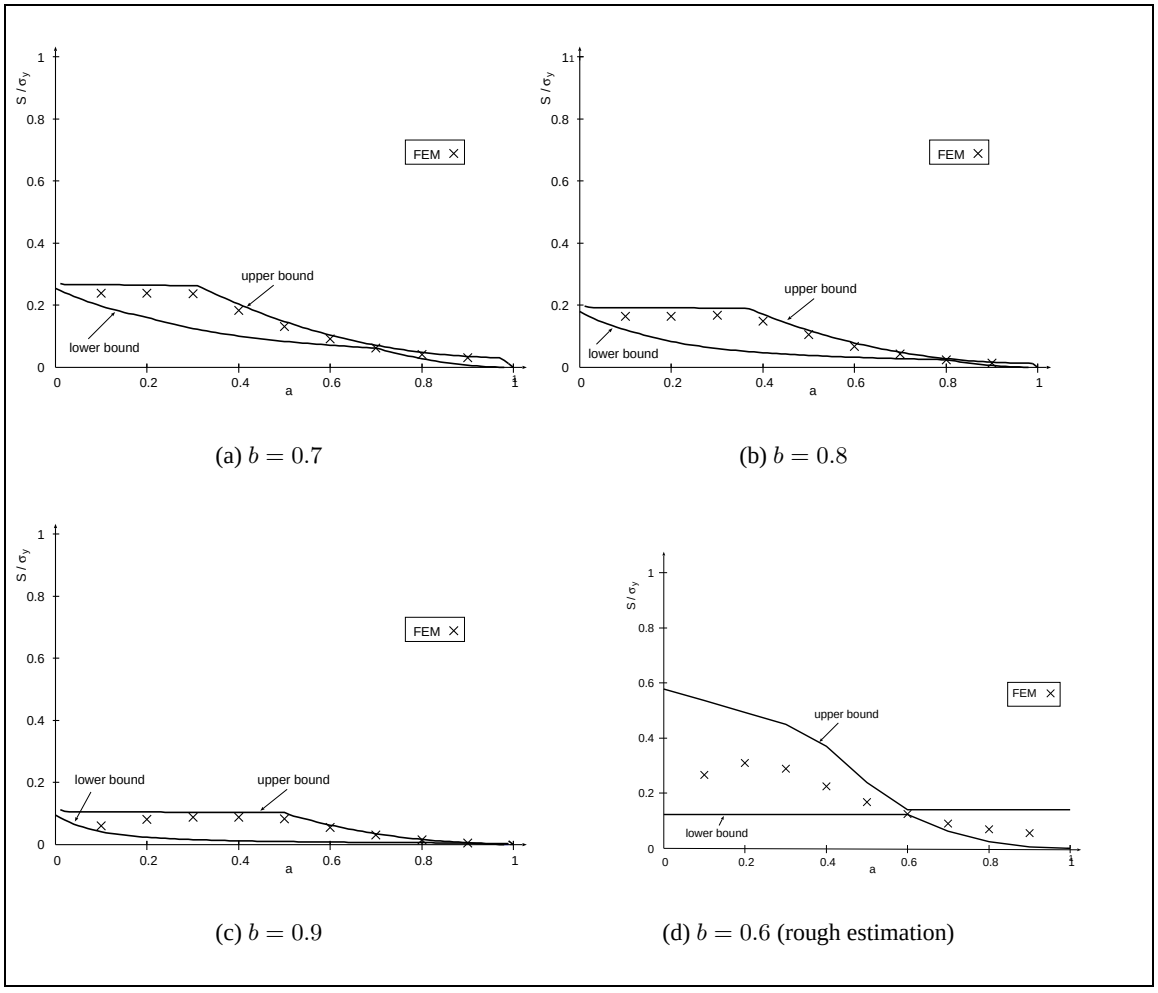

(a) $b = 0.7$

(b) $b = 0.8$

(c) $b = 0.9$

(d) $b = 0.6$ (rough estimation)

Figure 16: Comparison of lower and upper bounds for opposite biaxial loading with Finite Element calculations for constant b and rough estimation for $b = 0.6$

9. Conclusions

Plastic limit analysis for a square plate with a centered elliptical hole under uniaxial, equal biaxial and opposite biaxial tension loading has been presented. The load limits and possible collapse modes have been examined. As far as we know, no such detailed analytical limit analysis for this problem has been given before. The approach can be considered a straight forward development of the respective one of plastic limit analysis for plates with centered circular holes (compare [3], [8], [10]). The procedure appears useful in solving engineering problems for plates.

REFERENCES

1. S. Alexandrov, N. Chicanova, M. Kocak: Analytical yield load solution for overmatched center cracked tension specimen, *Engineering Fracture Mechanics*, **64** (1999), 383–399.
2. H. Amstutz, T. Seeger: Experimentelle und theoretische Untersuchungen zur Übertragbarkeit von Standard-J_R-Kurven auf bauteilähnliche Strukturen. DFG-Report FD-1/1995 (1995).
3. F.A. Gaydon, A.W. McCrum: A theoretical investigation on the yield point loading of a square plate with a central circular hole, *Journal of the Mechanics and Physics of Solids* **2** (1954), 156-169.
4. F.A. Gaydon: On the yield–point loading of a square plate with concentric circular hole, *Journal of the Mechanics and Physics of Solids* **2** (1954), 170–176.
5. M. Heitzer: Traglast– und Einspielanalyse zur Bewertung der Sicherheit passiver Komponenten. *Berichte des Forschungszentrums Jülich* **Jül–3704**, 1999.
6. M. Heitzer, G. Pop, M. Staat: Basis reduction for the shakedown problem for bounded kinematic hardening material, *Journal of Global Optimization* **17** (2000) 185–200.
7. M. Heitzer, M. Staat: FEM–computation of load carrying capacity of highly loaded passive components by direct methods. *Nuclear Engineering and Design* **193** (1999) 349–358.
8. R. Hill: *The Mathematical Theory of Plasticity*. Oxford University Press, Amen House, London, 1950.
9. R. Hill: On discontinuous plastic states, with special reference to localized necking in thin sheets,*Journal of the Mechanics and Physics of Solids* **1** (1952), 19–30.
10. P. G. Hodge: *Plastic Analysis of Structures*. McGraw–Hill, New York, 1959.
11. J. Joch, R.A. Ainsworth, T.H. Hyde: Limit load and J–estimates for idealised problems of deeply cracked welded joints in plane–strain bending and tension, *Fatigue and Fracture of Engineering Materials and Structures* **16** (1993) 1061–1079.
12. Maple 8 Getting Started Guide. Waterloo Maple Inc., Waterloo, ISBN 1-894511-25-5, 2002.
13. A. G. Miller: Review of Limit Loads of Structures Containing Defects. *International Journal of Pressure Vessel & Piping* **32** (1988) 197–327.
14. PERMAS User's Reference Manuals. Stuttgart: INTES Publications No. 202, 207, 208, 302, UM 404, UM 405, 1988.
15. M. Save: *Atlas of limit loads of Metal Plates, Shells and Disks*. Elsevier, Amsterdam, 1997.
16. K.-H. Schwalbe, U. Zerbst, Y.J. Kim, W. Brocks, A. Cornec, J. Heerens, H. Amstutz: *EFAM ETM97 – the ETM method for assessing the significance of crack-like defects in engineering structures, comprising versions ETM97/1 and ETM97/2.* Report GKSS 98/E/6, GKSS-Forschungszentrum Geesthacht, 1998.
17. M. Staat, M. Heitzer (eds.): *Numerical Methods for Limit and Shakedown Analysis.* NIC-Series Vol.15, John von Neumann Institute for Computing, Jülich, 2003.
18. M. Staat, M. Heitzer, A. Yan, V. Khoi, D. Nguyen, F. Voldoire, A. Lahousse: Limit Analysis of Defects. *Berichte des Forschungszentrums Jülich* **Jül-3746**, 2000.
19. E. Stein, G. Zhang, R. Mahnken: Shakedown analysis for perfectly plastic and kinematic hardening materials, in Stein, E. (ed.): *Progress in computational analysis of inelastic structures*, Wien, Springer, 175–244, 1993.